Available online at www.sciencedirect.com
ScienceDirect
Journal of Sound and Vibration 297 (2006) 931–945
JOURNAL OF SOUND AND VIBRATION
www.elsevier.com/locate/jsvi

Free vibration analysis of non-cylindrical helices with, variable cross-section by using mixed FEM

Konuralp Girgin*

Civil Engineering Faculty, Istanbul Technical University, Maslak, 34469, Istanbul, Turkey

Received 6 February 2006; received in revised form 26 April 2006; accepted 2 May 2006
Available online 30 June 2006

Abstract

The objective of the study is to present a mixed finite element (FE) formulation for the free vibration analysis of non-cylindrical helices with variable cross-section. Non-cylindrical helix geometry was well approximated through the variable arc lengths and linear variations in curvatures via shape functions. The mixed FE model for non-cylindrical helices was developed by using the exact cylindrical helix geometry and corresponding field equations. The element and consistent mass matrices are attained under these assumptions. The element matrix is derived based on the Timoshenko beam theory and the effects of rotary inertia are involved into the mass matrix. Although the formulation is quite simple, the generated element is capable to provide highly accurate solutions for the conical, barrel and hyperboloidal geometries of non-cylindrical helices. The results of presented FE model based on an approximated geometry approach are in a good agreement with the other studies in the actual literature. Some original examples were generated and solved for the literature as well.

1. Introduction

Helical springs have been evolved to meet needs in engineering practice especially in mechanical and civil engineering. They are significant elements in machines and vehicles and preferred at the stair applications in civil engineering due to the architectural requirements. Numerous theoretical, numerical and experimental investigations of helices are available in the literature. The first differential equations for helical spring dynamics were given by Love [1]. Epstein [2] theoretically derived both the elongations and fundamental frequencies of conical coil springs for several dynamic boundary conditions and experimentally verified the frequencies on nickel and piano wire springs. Love's [1] equations were extended by Yoshimura and Murata [3] by considering the torsional inertia effect. Young and Scordelis [4] investigated the accuracy of the theories by performing an experimental study. Scordelis [5] proposed general equations for the determination of the redundants at midspan of a uniformly loaded helicoidal girder fixed at its ends. He also obtained the internal forces for 510 different cases by including the variables being horizontal angle, angle of slope and cross-sectional dimensions. Neglecting the axial and shear deformations, Cinemre [6] statically solved the isotropic

*Corresponding author. Fax: +902122856587.
E-mail address: kgirgin@ins.itu.edu.tr.

0022-460X/$ - see front matter
doi:10.1016/j.jsv.2006.05.001

Nomenclature

A	cross-sectional area
$A' = A/k'$	shear area
$\bar{A}, \bar{K}, \bar{I}_t, \bar{I}_n, \bar{I}_b$	cross-sectional properties
$(\bar{A})_\beta, (\bar{K})_\beta, (\bar{I}_t)_\beta, (\bar{I}_n)_\beta, (\bar{I}_b)_\beta$, $(\beta = i,j)$	nodal values of cross-sectional properties
$(AE)_\beta$, $(GI_t)_\beta$, $(GI_n)_\beta$, $(GI_b)_\beta$ $(\beta = i,j)$	nodal values of the rigidities
c	$c = \sqrt{R^2 + p^2}$
c_i, c_j	nodal values of c
d_i, d_j	denotes the nodal variables at i and j nodes, respectively
$\mathrm{d}s = \sqrt{\mathrm{d}x^2 + \mathrm{d}y^2 + \mathrm{d}z^2}$	infinitesimal arc length in the cartesian coordinate system
E, G, v	Young's modulus, shear modulus, Poisson's ratio
$\mathbf{I}$	moment of inertia
i, j	represent node numbers of the finite element
$\mathbf{i}$, $\mathbf{j}$, $\mathbf{k}$	unit vectors in the directions of x, y and z axes, respectively
I_t	torsional moment of inertia
I_n, I_b	moments of inertia of cross-section with respect to normal and binormal axes, respectively
k′	shear coefficient
$[\mathbf{k}^{d_1,d_2}]$	sub-element matrix including d_1 and d_2 variables
$[\widehat{\boldsymbol{k}}]$	sub-element matrix including boundary conditions
$[\mathrm{m}^e]$	element mass matrix
$[m^{d_1,d_2}]$	sub-mass matrix including d_1 and d_2 variables
$\mathbf{M}$	moment vectors
n	number of active turns
p_i, p_j	nodal step for unit angles at i and j nodes, respectively
$p(\varphi)$	step for unit angle
$\mathbf{r}$	position vector
$R(\varphi)$	centerline radius varying with φ
$s^e = c\Delta\varphi$	helix finite element arc length
$\mathbf{t}$, $\mathbf{n}$, $\mathbf{b}$	are the tangential, normal and binormal unit vectors, respectively
$\mathbf{T}$	internal force vectors
$\mathbf{u}$	displacement vector in the centroid of cross-section
$\hat{\mathbf{u}}, \hat{\boldsymbol{\Omega}}, \hat{\mathbf{T}}, \hat{\mathbf{M}}$	the known boundary conditions
α	pitch angle
β	reduction factor for the cross-sectional diameter
$\boldsymbol{\gamma}$	shear unit angle vector
$\boldsymbol{\kappa}$	unit rotation vector
ρ	density of material
τ_i, τ_j	nodal torsions of the spring axis at i and j nodes, respectively
φ	horizontal angle
φ_i and φ_j	horizontal angle at i and j nodes, respectively
χ, τ	curvature and torsion of the helix axis
χ_i, χ_j	nodal curvatures of the spring axis at i and j nodes, respectively
ψ_i, ψ_j	linear shape functions at nodes i and j
$[(\ldots\ldots)]_\sigma$	geometric boundary conditions
$[(\ldots\ldots)]_\tau$	dynamic boundary conditions
ω	angular frequency
$\boldsymbol{\Omega}$	rotational vector around the centroidal axes of cross-section

cylindrical helices by an exact solution technique for the so-called carry-over (transfer) matrix. Wittrick [7] worked out the wave propagation in semi-infinite springs and obtained approximate solutions by considering the rotary inertia and shear deformations.

Finite element (FE) technique is widely used in the analysis of helicoidal springs due to its flexibility in applications. Mottershead [8] studied the dynamics of the helical rods and springs. His formulation suggested in his work also confirmed Wittrick's [7] equations exactly. The natural frequencies according to his method were in a good agreement with his experimental study. Using Wittrick's [7] differential equations Mottershead [9] extended the theory to large displacement theory through Lagrange–Green strain equations and derived consistent geometric stiffness matrices. He offered an investigation of static, dynamic stability and nonlinear wave propagation of springs. Using the Myklestad method, Nagaya et al. [10] studied the free vibration analysis for barrel and hyperboloidal types of helical springs numerically and experimentally. Pearson and Wittrick [11] developed a theory for the uniform helical springs based on the Bernoulli–Euler beam theory to derive the dynamic stiffness matrix by considering steady-state and steady-state forced vibration. Based on the Timoshenko theory Akoz et al. [12] developed a functional, for the static analysis, suitable to the mixed FE equations and applicable to three dimensional bars with arbitrary geometry and variable cross-section.

Omurtag and Akoz [13] analyzed helical beams with variable cross-section under arbitrary static loading by using mixed FE where shear effects were considered. Xiong and Tabarrok [14] developed a general element for the vibration analysis of spatially curved and twisted rods under various loads. They considered the initial bending moments, shear forces as well as axial loads and stated that the element could be used for the vibration analysis of rods subjected to conservative and non-conservative follower-type forces. Yıldırım [15] developed a numerical algorithm by determining the static element transfer matrix and studied the parameters affecting the free vibration frequency of helical springs, in which shear effect and torsional moments of inertia were considered. Employing the transfer method and the complementary functions Yıldırım and Ince [16] determined the free vibration frequencies of non-cylindrical helices by including the effects of rotary inertia, shear and axial deformations. Yıldırım [17] used the distributed parameter model for the free vibration analysis of non-cylindrical helices and derived the exact natural frequencies for circular and squared sections in graphical forms. Yıldırım [18] presented analytical expressions for the first six natural frequencies of isotropic cylindrical helical springs with circular or rectangular cross-sections. Lee and Thompson [19] obtained the dynamic stiffness matrix through the equation of free wave motion in helical spring based on the Timoshenko beam theory and calculated the natural frequencies by means of Wittrick–Williams method. Employing the transfer matrix method Becker et al. [20] produced the frequency design charts of helical compression springs with circular cross-section and clamped ends. Busool and Eisenberger [21] attained the exact shape functions having terms less than 200 to derive the dynamic stiffness matrix of arbitrary shaped helices with variable cross-section by considering the effects of axial, shear deformations and the rotary inertia.

This study presents a method with respect to FEM analysis for non-cylindrical, variable cross-sectional helices by including the variation of curvatures and arc lengths. As far as the author's knowledge, this research is the first study on the free vibration analysis of non-cylindrical helices with variable cross-sections. This method was developed based on the functional introduced by Omurtag and Akoz [13] for the static analyses of the cylindrical helices with exact geometry. According to the developed method in this study, the consistent mass matrix encompasses the rotatory inertia and the effects of torsional moment of inertia while mixed FE matrix considers the shear effect. Although the proposed approach is quite simple, the results are in an excellent agreement with the FEM results based on exact geometry in the literature, when compared with regard to precision and number of elements. The results were verified through the studies in the actual literature and ANSYS [22]. Finally, original examples were generated and solved for the literature as well.

2. Field equations and functional

In this study, the helices made of elastic, isotropic-homogenous material are considered by regarding first-order theory and warping is neglected.

2.1. Non-cylindrical helix geometry

The geometrical properties of the non-cylindrical helix in Fig. 1 are given:

$$x = R(\varphi)\cos(\alpha), \quad y = R(\varphi)\sin(\alpha), \quad z = p(\varphi)\varphi, \tag{1}$$

$$p(\varphi) = R(\varphi)\tan(\alpha), \tag{2}$$

where α denotes the pitch angle, $R(\varphi)$ and $p(\varphi)$ signify the centerline radius and the step for unit angle of the helix as a function of the horizontal angle φ, respectively. In the cartesian coordinate system, the position vector of any point on a helix can be expressed as $\mathbf{r} = x\mathbf{i} + y\mathbf{j} + z\mathbf{k}$ via the unit vectors $\mathbf{i}$, $\mathbf{j}$, $\mathbf{k}$ in the directions of x, y and z axes, respectively. In the Frenet coordinate system, as seen in Fig. 2, unit Frenet vectors differentially depends on the position vector $\mathbf{r}$ in the form

$$\mathbf{t} = \frac{\mathrm{d}\mathbf{r}}{\mathrm{d}s}, \quad \mathbf{n} = \frac{\mathrm{d}\mathbf{t}/\mathrm{d}s}{\left\|\mathrm{d}\mathbf{t}/\mathrm{d}s\right\|}, \quad \mathbf{b} = \mathbf{t} \times \mathbf{n}, \tag{3}$$

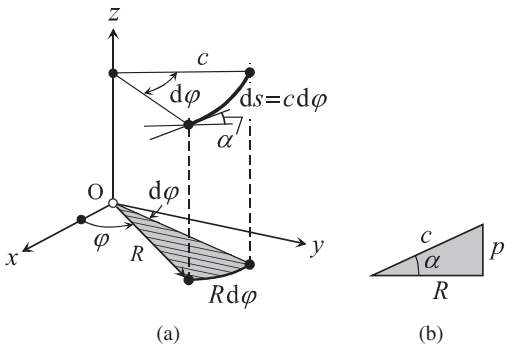

Fig. 1. Some geometrical properties of helix.

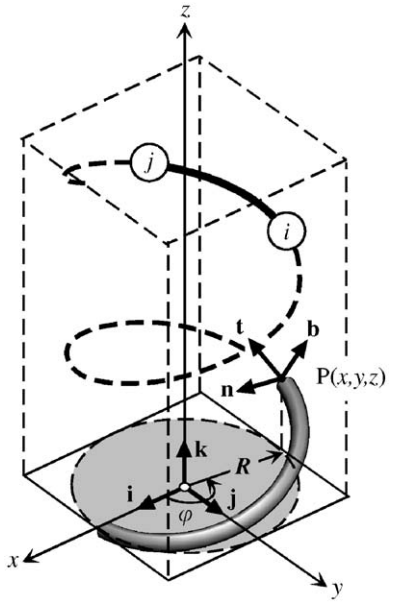

Fig. 2. Cartesian and Frenet axes of a helix.

where **t**, **n**, **b** are the tangential, normal and binormal unit vectors, respectively, and the infinitesimal arc length ds in the cartesian coordinate system is $ds = \sqrt{dx^2 + dy^2 + dz^2}$. In the Frenet coordinate system,

$$ds = \sqrt{R^2(\varphi) + p^2(\varphi)}\, d\varphi = c(\varphi)\, d\varphi, \tag{4}$$

$$\frac{d\mathbf{t}}{ds} = \chi\mathbf{n}, \quad \frac{d\mathbf{n}}{ds} = -\chi\mathbf{t} + \tau\mathbf{b}, \quad \frac{d\mathbf{b}}{ds} = -\tau\mathbf{n}, \tag{5}$$

where χ and τ are the curvature and torsion of the helix axis, respectively, according to Omurtag [23].

2.2. Cylindrical helix geometry

In the case of cylindrical helix, since centerline radius of helix is $R = R(\varphi) = \text{constant}$, all the variables are constant and

$$\chi = \frac{R}{c^2}, \quad \tau = \frac{p}{c^2}, \quad c^2 = R^2 + p^2, \quad p = R\tan\alpha. \tag{6}$$

The transformation matrices of unit vectors between the cartesian and Frenet co-ordinate systems are:

$$\begin{Bmatrix} \mathbf{i} \\ \mathbf{j} \\ \mathbf{k} \end{Bmatrix} = \begin{bmatrix} -\frac{R}{c}\sin\varphi & -\cos\varphi & \frac{p}{c}\sin\varphi \\ \frac{R}{c}\cos\varphi & -\sin\varphi & \frac{p}{c}\cos\varphi \\ -\frac{p}{c} & 0 & \frac{R}{c} \end{bmatrix} \begin{Bmatrix} \mathbf{t} \\ \mathbf{n} \\ \mathbf{b} \end{Bmatrix}, \tag{7}$$

$$\begin{Bmatrix} \mathbf{t} \\ \mathbf{n} \\ \mathbf{b} \end{Bmatrix} = \begin{bmatrix} -\frac{R}{c}\sin\varphi & \frac{R}{c}\cos\varphi & \frac{p}{c}\sin\varphi \\ -\cos\varphi & -\sin\varphi & 0 \\ \frac{p}{c}\sin\varphi & -\frac{p}{c}\cos\varphi & \frac{R}{c} \end{bmatrix} \begin{Bmatrix} \mathbf{i} \\ \mathbf{j} \\ \mathbf{k} \end{Bmatrix}. \tag{8}$$

2.3. Field equations in cylindrical helix

The vectorial quantities $\mathbf{u}$, Ω, $\mathbf{T}$ and $\mathbf{M}$ are expressed in Frenet coordinate axes as follows:

$$\left.\begin{aligned} \mathbf{u} &= u_t\mathbf{t} + u_n\mathbf{n} + u_b\mathbf{b} \\ \mathbf{\Omega} &= \Omega_t\mathbf{t} + \Omega_n\mathbf{n} + \Omega_b\mathbf{b} \\ \mathbf{T} &= T_t\mathbf{t} + T_n\mathbf{n} + T_b\mathbf{b} \\ \mathbf{M} &= M_t\mathbf{t} + M_n\mathbf{n} + M_b\mathbf{b} \end{aligned}\right\}, \tag{9}$$

where $\mathbf{u}$ is the displacement vector in the centroid of the cross-section, Ω is the rotational vector around the centroidal axes of the cross-section, $\mathbf{T}$ and $\mathbf{M}$ are the internal force and the moment vectors, respectively. Field equations of the Timoshenko beam [24] are:

$$\text{Equation of motion}: \quad \left.\begin{aligned} \tfrac{\mathrm{d}\mathbf{T}}{\mathrm{d}s} - \rho A\ddot{\mathbf{u}} + \mathbf{p} &= \mathbf{0} \\ \tfrac{\mathrm{d}\mathbf{M}}{\mathrm{d}s} + \mathbf{t}\times\mathbf{T} - \rho\mathbf{I}\ddot{\mathbf{\Omega}} + \mathbf{m} &= \mathbf{0} \end{aligned}\right\}, \tag{10}$$

$$\text{Kinematic equations}: \quad \left.\begin{aligned} \boldsymbol{\gamma} - \tfrac{\mathrm{d}\mathbf{u}}{\mathrm{d}s} - \mathbf{t}\times\mathbf{\Omega} &= \mathbf{0} \\ \boldsymbol{\kappa} - \tfrac{\mathrm{d}\mathbf{\Omega}}{\mathrm{d}s} &= \mathbf{0} \end{aligned}\right\}, \tag{11}$$

$$\text{Constitutive equations}: \quad \left.\begin{aligned} \mathbf{C}_\gamma\mathbf{T} - \boldsymbol{\gamma} &= \mathbf{0} \\ \mathbf{C}_\kappa\mathbf{M} - \boldsymbol{\kappa} &= \mathbf{0} \end{aligned}\right\}, \tag{12}$$

where $\ddot{\mathbf{u}} = \partial^2\mathbf{u}/\partial t^2$, $\boldsymbol{\gamma}$ is the shear unit angle vector, $\boldsymbol{\kappa}$ is the unit rotation vector, A is the cross-sectional area and $\mathbf{I}$ is the moment of inertia. Compliance matrices for homogenous-isotropic material according to Hooke's law are:

$$\mathbf{C}_\gamma = \begin{bmatrix} 1/EA & 0 & 0 \\ 0 & 1/GA' & 0 \\ 0 & 0 & 1/GA' \end{bmatrix}, \quad \mathbf{C}_\kappa = \begin{bmatrix} 1/EI_t & 0 & 0 \\ 0 & 1/EI_n & 0 \\ 0 & 0 & 1/EI_b \end{bmatrix}, \tag{13}$$

where E and G are Young's modulus and shear modulus, respectively, $A' = A/k'$ is the shear area, k' is the shear coefficient, I_t is the torsional moment of inertia, I_n and I_b moments of inertia around the $\mathbf{n}$ and $\mathbf{b}$ axes, respectively.

2.4. Functional

Using the Gâteaux differential Akoz et al. [12] developed a functional suitable to the mixed FEM formulation. Later, Omurtag and Akoz [13] employed this functional for the static analysis of cylindrical helices in Fig. 2. Instead of equilibrium equations, from Eq. (10) and for $\mathbf{p} = \mathbf{m} = \mathbf{0}$, this functional yields,

$$\left.\begin{aligned} I(\mathbf{y}) = &-\left[\mathbf{u}, \tfrac{\mathrm{d}\mathbf{T}}{\mathrm{d}s}\right] + [\mathbf{t}\times\mathbf{\Omega}, \mathbf{T}] - \left[\tfrac{\mathrm{d}\mathbf{M}}{\mathrm{d}s}, \mathbf{\Omega}\right] - \tfrac{1}{2}[\mathbf{C}_\kappa\mathbf{M}, \mathbf{M}] - \tfrac{1}{2}[\mathbf{C}_\gamma\mathbf{T}, \mathbf{T}] \\ &-\tfrac{1}{2}\rho A\omega^2[\mathbf{u}, \mathbf{u}] - \tfrac{1}{2}\rho\omega^2[\mathbf{I}\mathbf{\Omega}, \mathbf{\Omega}] \\ &+[(\mathbf{T} - \hat{\mathbf{T}}, \mathbf{u})]_\sigma + [(\mathbf{M} - \hat{\mathbf{M}}, \mathbf{u})]_\sigma + [\hat{\mathbf{u}}, \mathbf{T}]_\varepsilon + [\hat{\mathbf{\Omega}}, \mathbf{M}]_\varepsilon \end{aligned}\right\}, \tag{14}$$

which is applicable to linear dynamic analysis. In Eq. (14) ρ is the density of material, ω is the angular frequency. $\hat{\mathbf{u}}, \hat{\mathbf{\Omega}}, \hat{\mathbf{T}}, \hat{\mathbf{M}}$ are the known boundary conditions. The σ and τ subscripts denote the geometric and dynamic boundary conditions, respectively.

3. Finite element formulation

3.1. Finite element matrices

Linear interpolation functions are used for the FE formulation

$$\psi_i = \frac{\varphi_j - \varphi}{\Delta\varphi}, \quad \psi_j = \frac{\varphi - \varphi_i}{\Delta\varphi}, \quad (\varphi_i \leqslant \varphi \leqslant \varphi_j), \tag{15}$$

where i and j indices represent node numbers of the FE as seen in Fig 2, $\varphi_j > \varphi_i$ and $\Delta\varphi = \varphi_j - \varphi_i$. In the case of cylindrical helix FE, arc length is $s^e = c\Delta\varphi$ where c is constant. The main objective of this study is to derive the element and mass matrices which are applicable to non-cylindrical helices using the equations of exact cylindrical geometry as well as the variable cross-sectional properties. Approximating the non-cylindrical geometry will be achieved by means of the shape functions, as given below:

$$\left.\begin{aligned} c^e &= c_i\psi_i + c_j\psi_j \\ s^e &= (c_i\psi_i + c_j\psi_j)\Delta\varphi \\ \tau^e &= \tau_i\psi_i + \tau_j\psi_j \\ \chi^e &= \chi_i\psi_i + \chi_j\psi_j \end{aligned}\right\}. \tag{16}$$

For all the nodes of i and j the variables p_i, p_j, c_i, c_j, χ_i, χ_j, τ_i, τ_j are calculated through Eq. (6) where R_i and R_j are the radii of helices. Formulation of the variable cross-section will be achieved, as stated by Omurtag and Akoz [13], in the form,

$$\left.\begin{aligned} \bar{A}(\varphi) &= \tfrac{1}{(AE)_i}\psi_i + \tfrac{1}{(AE)_j}\psi_j \\ \bar{K}(\varphi) &= \tfrac{1}{(GA')_i}\psi_i + \tfrac{1}{(GA')_j}\psi_j \\ \bar{I}_t(\varphi) &= \tfrac{1}{(GI_t)_i}\psi_i + \tfrac{1}{(GI_t)_j}\psi_j \\ \bar{I}_n(\varphi) &= \tfrac{1}{(GI_n)_i}\psi_i + \tfrac{1}{(GI_n)_j}\psi_j \\ \bar{I}_b(\varphi) &= \tfrac{1}{(GI_b)_i}\psi_i + \tfrac{1}{(GI_b)_j}\psi_j \end{aligned}\right\}, \tag{17}$$

where $(AE)_i$, $(AE)_j$, … , $(GI_b)_i$, $(GI_b)_j$ are nodal values of the rigidities. Finally the mixed element matrix becomes,

$$[\mathrm{k}^e] = \left[\begin{array}{cccccc:cccccc} \mathbf{0} & \mathbf{0} & \mathbf{0} & \mathbf{0} & \mathbf{0} & \mathbf{0} & [\hat{\mathrm{k}}] & [\mathrm{k}^{c,\chi}] & \mathbf{0} & \mathbf{0} & \mathbf{0} & \mathbf{0} \\ & \mathbf{0} & \mathbf{0} & \mathbf{0} & \mathbf{0} & \mathbf{0} & -[\mathrm{k}^{c,\chi}] & [\hat{\mathrm{k}}] & [\mathrm{k}^{c,\tau}] & \mathbf{0} & \mathbf{0} & \mathbf{0} \\ & & \mathbf{0} & \mathbf{0} & \mathbf{0} & \mathbf{0} & \mathbf{0} & -[\mathrm{k}^{c,\tau}] & [\hat{\mathrm{k}}] & \mathbf{0} & \mathbf{0} & \mathbf{0} \\ & & & \mathbf{0} & \mathbf{0} & \mathbf{0} & \mathbf{0} & \mathbf{0} & \mathbf{0} & [\hat{\mathrm{k}}] & [\mathrm{k}^{c,\chi}] & \mathbf{0} \\ & & & & \mathbf{0} & \mathbf{0} & \mathbf{0} & \mathbf{0} & [\mathrm{k}^{c}] & -[\mathrm{k}^{c,\chi}] & [\hat{\mathrm{k}}] & [\mathrm{k}^{c,\tau}] \\ & & & & & \mathbf{0} & \mathbf{0} & -[\mathrm{k}^{c}] & \mathbf{0} & \mathbf{0} & -[\mathrm{k}^{c,\tau}] & [\hat{\mathrm{k}}] \\ \hdashline & & & & & & -[\mathrm{k}^{c,\bar{A}}] & \mathbf{0} & \mathbf{0} & \mathbf{0} & \mathbf{0} & \mathbf{0} \\ & & & & & & & -[\mathrm{k}^{c,\bar{K}}] & \mathbf{0} & \mathbf{0} & \mathbf{0} & \mathbf{0} \\ & & & & & & & & -[\mathrm{k}^{c,\bar{K}}] & \mathbf{0} & \mathbf{0} & \mathbf{0} \\ & & & & & & & & & -[\mathrm{k}^{c,\bar{I}_t}] & \mathbf{0} & \mathbf{0} \\ & & & & & & & \textit{symmetrical} & & & -[\mathrm{k}^{c,\bar{I}_n}] & \mathbf{0} \\ & & & & & & & & & & & -[\mathrm{k}^{c,\bar{I}_b}] \end{array}\right], \tag{18}$$

where the nodal variable vector for the element matrix in Eq. (18) is

$$\mathbf{X}^{\mathrm{T}} = \{u_t\ u_n\ u_b\ \Omega_t\ \Omega_n\ \Omega_b\ T_t\ T_n\ T_b\ M_t\ M_n\ M_b\}.$$

Dimensions of all the square sub-matrices in Eq. (18) are 2×2. Boundary conditions are given in the following matrix:

$$[\widehat{k}] = \begin{bmatrix} 0.5 & -0.5 \\ 0.5 & -0.5 \end{bmatrix}. \tag{19}$$

The superscript indices used in the square sub-matrices $[\mathbf{k}^{c,\bar{A}}]$, $[\mathbf{k}^{c,\bar{K}}]$, $[\mathbf{k}^{c,\bar{I}_t}]$, $[\mathbf{k}^{c,\bar{I}_n}]$, $[\mathbf{k}^{c,\bar{I}_b}]$, $[\mathbf{k}^{c}]$, $[\mathbf{k}^{c,\chi}]$, $[\mathbf{k}^{c,\tau}]$ indicate the variation of helix geometry (c, χ, τ) and the cross-sectional properties $(\bar{A}, \bar{K}, \bar{I}_t, \bar{I}_n, \bar{I}_b)$. The terms of the sub-matrices including two variables are:

$$\left.\begin{aligned} k_{ii}^{c,d} &= \tfrac{1}{60}\Delta\varphi[3c_i(4d_i + d_j) + c_j(3d_i + 2d_j)] \\ k_{ij}^{c,d} &= k_{ji}^{c,d} = \tfrac{1}{60}\Delta\varphi[c_i(3d_i + 2d_j) + c_j(2d_i + 3d_j)] \\ k_{jj}^{c,d} &= \tfrac{1}{60}\Delta\varphi[c_i(2d_i + 3d_j) + 3c_j(d_i + 4d_j)] \end{aligned}\right\}, \tag{20}$$

where the variable d_i, d_j denote the nodal values of χ_β, τ_β and $(\bar{A})_\beta, (\bar{K})_\beta, (\bar{I}_t)_\beta, (\bar{I}_n)_\beta, (\bar{I}_b)_\beta$, $(\beta = i,j)$. In the case of $d_i = d_j = d =$ constant the above equations become

$$\left.\begin{aligned} k_{ii}^{c} &= \tfrac{1}{12}d\,\Delta\varphi(3c_i + c_j) \\ k_{ij}^{c} &= k_{ji}^{c} = \tfrac{1}{12}d\,\Delta\varphi(c_i + c_j) \\ k_{jj}^{c} &= \tfrac{1}{12}d\,\Delta\varphi(c_i + 3c_j) \end{aligned}\right\}. \tag{21}$$

Variable cross-sectional properties of a helix can be expressed as

$$\left.\begin{aligned} \widetilde{A}(\varphi) &= A_i\psi_i + A_j\psi_j, & \widetilde{I}_n(\varphi) &= (I_n)_i\psi_i + (I_n)_j\psi_j \\ \widetilde{I}_t(\varphi) &= (I_t)_i\psi_i + (I_t)_j\psi_j, & \widetilde{I}_b(\varphi) &= (I_b)_i\psi_i + (I_b)_j\psi_j \end{aligned}\right\}, \tag{22}$$

where $A_\beta\ ,(\beta = i,j)$ and $(I_t, I_n, I_b)_\beta\ ,(\beta = i,j)$ are the nodal values of cross-sectional areas, torsional moment of inertia and moment of inertias around principles axes of cross-section, respectively. By means of Eqs. (16), (20) and (22) the mass matrix considering the approximated geometry of non-cylindrical helix becomes

$$[\mathrm{m}^e] = \left[\begin{array}{cccccc:cccccc} [\mathrm{m}^{c,\tilde{A}}] & \mathbf{0} & \mathbf{0} & \mathbf{0} & \mathbf{0} & \mathbf{0} & \mathbf{0} & \mathbf{0} & \mathbf{0} & \mathbf{0} & \mathbf{0} & \mathbf{0} \\ & [\mathrm{m}^{c,\tilde{A}}] & \mathbf{0} & \mathbf{0} & \mathbf{0} & \mathbf{0} & \mathbf{0} & \mathbf{0} & \mathbf{0} & \mathbf{0} & \mathbf{0} & \mathbf{0} \\ & & [\mathrm{m}^{c,\tilde{A}}] & \mathbf{0} & \mathbf{0} & \mathbf{0} & \mathbf{0} & \mathbf{0} & \mathbf{0} & \mathbf{0} & \mathbf{0} & \mathbf{0} \\ & & & [\mathrm{m}^{c,\tilde{I}_t}] & \mathbf{0} & \mathbf{0} & \mathbf{0} & \mathbf{0} & \mathbf{0} & \mathbf{0} & \mathbf{0} & \mathbf{0} \\ & & & & [\mathrm{m}^{c,\tilde{I}_n}] & \mathbf{0} & \mathbf{0} & \mathbf{0} & \mathbf{0} & \mathbf{0} & \mathbf{0} & \mathbf{0} \\ & & & & & [\mathrm{m}^{c,\tilde{I}_b}] & \mathbf{0} & \mathbf{0} & \mathbf{0} & \mathbf{0} & \mathbf{0} & \mathbf{0} \\ \hdashline & & & & & & \mathbf{0} & \mathbf{0} & \mathbf{0} & \mathbf{0} & \mathbf{0} & \mathbf{0} \\ & & & & & & & \mathbf{0} & \mathbf{0} & \mathbf{0} & \mathbf{0} & \mathbf{0} \\ & & & & & & & & \mathbf{0} & \mathbf{0} & \mathbf{0} & \mathbf{0} \\ & & & & & & & & & \mathbf{0} & \mathbf{0} & \mathbf{0} \\ & & \textit{symmetrical} & & & & & & & & \mathbf{0} & \mathbf{0} \\ & & & & & & & & & & & \mathbf{0} \end{array}\right], \tag{23}$$

where all the 2×2 sub-matrices, which are handled in a similar way given by Eq. (20), are in the form,

$$\left.\begin{aligned} m_{ii}^{c,d} &= \tfrac{1}{60}\rho\Delta\varphi[3c_i(4d_i + d_j) + c_2(3d_i + 2d_j)] \\ m_{ij}^{c,d} &= m_{ji}^{c,d} = \tfrac{1}{60}\rho\Delta\varphi[c_i(3d_i + 2d_j) + c_j(2d_i + 3d_j)] \\ m_{jj}^{c,d} &= \tfrac{1}{60}\rho\Delta\varphi[c_i(2d_i + 3d_j) + 3c_j(d_i + 4d_j)] \end{aligned}\right\}. \tag{24}$$

3.2. Solution method in the FEM

Free vibration analysis in the FEM can be expressed as

$$([\mathbf{K}] - \omega^2[\mathbf{M}])\{\mathbf{w}\} = \{\mathbf{0}\} \tag{25}$$

and this analysis transforms into the standard solution of eigenvalue problem, where ω represents the natural angular frequencies, [**K**] denotes the system matrix, [**M**] is the mass matrix and **w** (**u**,**Ω**) signifies the column

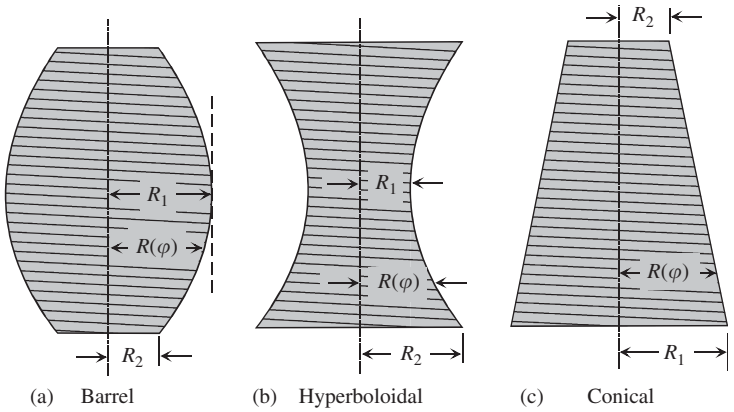

Fig. 3. Radii of non-cylindrical helices.

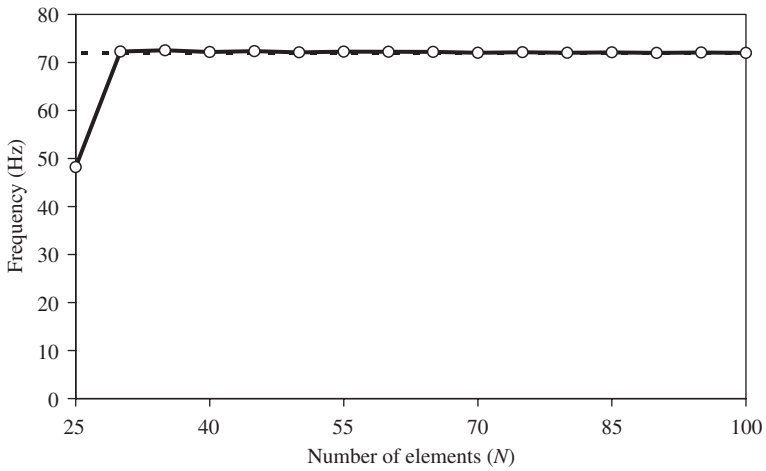

Fig. 4. The convergence of the first natural frequency of barrel helix ($R_2/R_1 = 0.2$)with respect to the number of elements (Example 1), (○) This study, (- -) Ref. [16].

matrix including nodal displacements and rotations. In the mixed FEM, due to the nodal force and moment vector{**F**}, Eq. (25) is in the form

$$\left(\begin{bmatrix}[\mathbf{K}_{11}] & [\mathbf{K}_{12}]\\ [\mathbf{K}_{21}] & [\mathbf{K}_{22}]\end{bmatrix} - \omega^2\begin{bmatrix}[\mathbf{0}] & [\mathbf{0}]\\ [\mathbf{0}] & [\mathbf{M}]\end{bmatrix}\right)\begin{Bmatrix}\{\mathbf{F}\}\\ \{\mathbf{w}\}\end{Bmatrix} = \begin{Bmatrix}\{\mathbf{0}\}\\ \{\mathbf{0}\}\end{Bmatrix}. \tag{26}$$

Eliminating {**F**} from the above equation, the equation system reduces to

$$\left([\mathbf{K}^*] - \omega^2[\mathbf{M}]\right)\{\mathbf{w}\} = \{\mathbf{0}\}, \tag{27}$$

where $[\mathbf{K}^*] = [\mathbf{K}_{22}] - [\mathbf{K}_{12}]^{\mathrm{T}}[\mathbf{K}_{11}]^{-1}[\mathbf{K}_{12}]$ is the condensed system matrix.

4. Examples

The first and second examples, inspired by the literature, are on the free vibration analysis of non-cylindrical helices with constant cross-section based on the exact geometry introduced by Nagaya et al. [10], Yıldırım and Ince [16]. Firstly; the approximated geometry approach were verified for these helices, and secondly variable cross-section case was considered by leading to original examples for the literature. Third example is a conical helix with variable rectangular cross-section along its centroidal axis. All the results have been compared either by the studies in literature or ANSYS [22].

Table 1
Natural frequencies (in Hz) of barrel type spring with constant circular cross-section ($d = 2$ mm, $R_2/R_1 = 0.2$, N: number of elements)

Mod	Nagaya et al. (theoretical) [10]	Yıldırım–Ince [16]	ANSYS [22]			This study			
	$N = 78$	$N = 50$	$N = 100$	$N = 500$	$N = 1000$	$N = 100$	$N = 75$	$N = 50$	$N = 30$
1	71.00	71.88	73.65	72.06	72.01	71.95	72.12	72.07	72.28
2	81.00	81.22	83.60	81.82	81.76	81.22	81.24	81.28	81.41
3	—	99.98	102.31	100.34	100.24	99.99	99.95	99.00	85.62
4	—	99.99	102.35	100.41	100.31	100.02	100.01	99.04	85.65
5	143.00	143.93	148.05	144.85	144.75	143.95	144.04	143.93	134.52
6	150.00	145.13	150.60	146.38	146.22	145.11	145.01	144.51	134.64

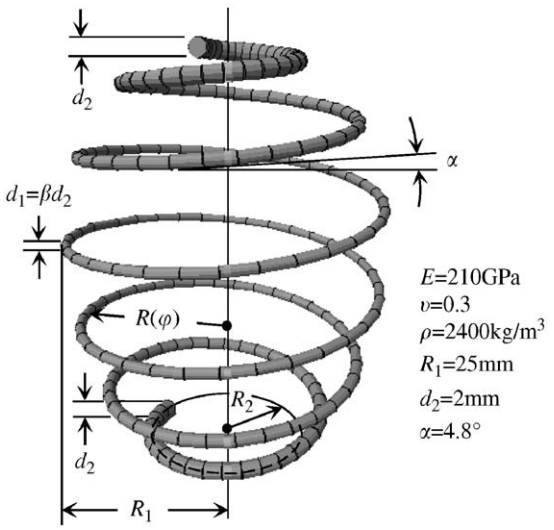

Fig. 5. Perspective view of barrel spring with variable circular cross-section.

Herein, the horizontal radius of any point on the centroidal axis of helix (see Figs. 5, 7 and 9) is determined using the following formulae:

$$\text{Barrel or hyperboloidal helices}: \quad R(\varphi) = R_1 + (R_2 - R_1)\left(1 - \frac{\varphi}{n\pi}\right)^2.$$

$$\text{Conical helices}: \quad R(\varphi) = R_1 + \frac{(R_2 - R_1)\varphi}{2n\pi},$$

where φ is the horizontal angle and n is the number of active turns of helix, respectively.

4.1. Example 1—barrel helix

Constant cross-section case: Geometrical and material properties of barrel helix (Fig. 3), fixed at both ends, are as the follows: the number of active turns $n = 6.5$, diameter $d = 2\,\text{mm}$, $R_1 = 25\,\text{mm}$, R_2 is variable, pitch angle $\alpha = 4.8^\circ$,Young modulus $E = 210\,\text{GPa}$, $\upsilon = 0.3$, $\rho = 7850\,\text{kg/m}^3$ and shear area coefficients $\alpha_n = \alpha_b = 1.1$. This problem was analyzed for the case of constant circular cross-section with $d = 2\,\text{mm}$. For $R_2/R_1 = 0.2$, the convergence of first natural frequency with respect to the elements number was given in Fig. 4. First six natural frequencies were compared with the studies by Nagaya et al. [10], Yildirim and Ince [16] and by ANSYS as well. The results were tabulated in Table 1.

Variable cross-section case: As far as the author's knowledge, variable cross-sectional barrel helix is an original evolution for the literature. Geometrical and material properties of the barrel helix in Fig. 5 are the same as the constant cross-section case. The diameter of circular cross-sections is equal to $d_2 = 2\,\text{mm}$ at the points $R = R_2$ and reduces linearly to βd_2 at $R = R_1$. Diameter variations were investigated for each values of β, where $\beta = 0.25$,0.50 and 0.75. The first six natural frequencies for the case of $R_2/R_1 = 0.2$ given in Table 2 were compared with the ANSYS. The proposed method in this study provides sufficient consistency via 100 elements, while ANSYS requires much more elements. The variations of the first six natural frequencies for $\beta = 0.25$,0.50,0.75,1.00 and $R_2/R_1 = 0.1,\ldots,1.0$ having an increment of 0.1 were illustrated in Fig. 6.

Table 2
Natural frequencies (in Hz) of barrel type spring with variable circular cross-section ($d_2 = 2\,\text{mm}$, $d_1 = \beta\, d_2$, $R_2/R_1 = 0.2$, N: number of elements)

β	Mod	ANSYS [22]			This study			
		$N = 100$	$N = 500$	$N = 1000$	$N = 100$	$N = 75$	$N = 50$	$N = 30$
	1	66.42	64.94	64.89	64.82	65.06	64.98	65.22
	2	71.21	69.63	69.58	69.24	69.39	69.36	69.55
0.75	3	89.22	87.46	87.38	87.19	87.28	86.40	74.85
	4	89.23	87.48	87.40	87.22	87.33	86.44	74.86
	5	120.28	117.59	117.50	116.86	117.02	116.93	111.10
	6	123.54	119.83	119.68	118.91	118.98	118.50	111.18
	1	55.58	54.31	54.26	54.13	54.37	54.28	54.47
	2	57.20	55.88	55.83	55.71	55.96	55.86	56.07
0.50	3	73.26	71.78	71.71	71.57	71.75	71.01	61.89
	4	73.32	71.82	71.75	71.63	71.82	71.09	61.96
	5	89.38	87.28	87.21	86.77	86.95	86.77	83.48
	6	92.93	90.14	90.02	89.54	89.69	89.26	83.97
	1	37.54	36.65	36.62	36.52	36.71	36.60	36.66
	2	40.60	39.63	39.59	39.53	39.76	39.63	39.69
0.25	3	49.24	48.16	48.12	47.96	48.13	47.85	44.07
	4	51.52	50.40	50.35	50.28	50.52	50.06	44.71
	5	54.89	53.51	53.45	53.22	53.37	53.09	50.27
	6	57.58	55.94	55.87	55.66	55.84	55.48	52.05

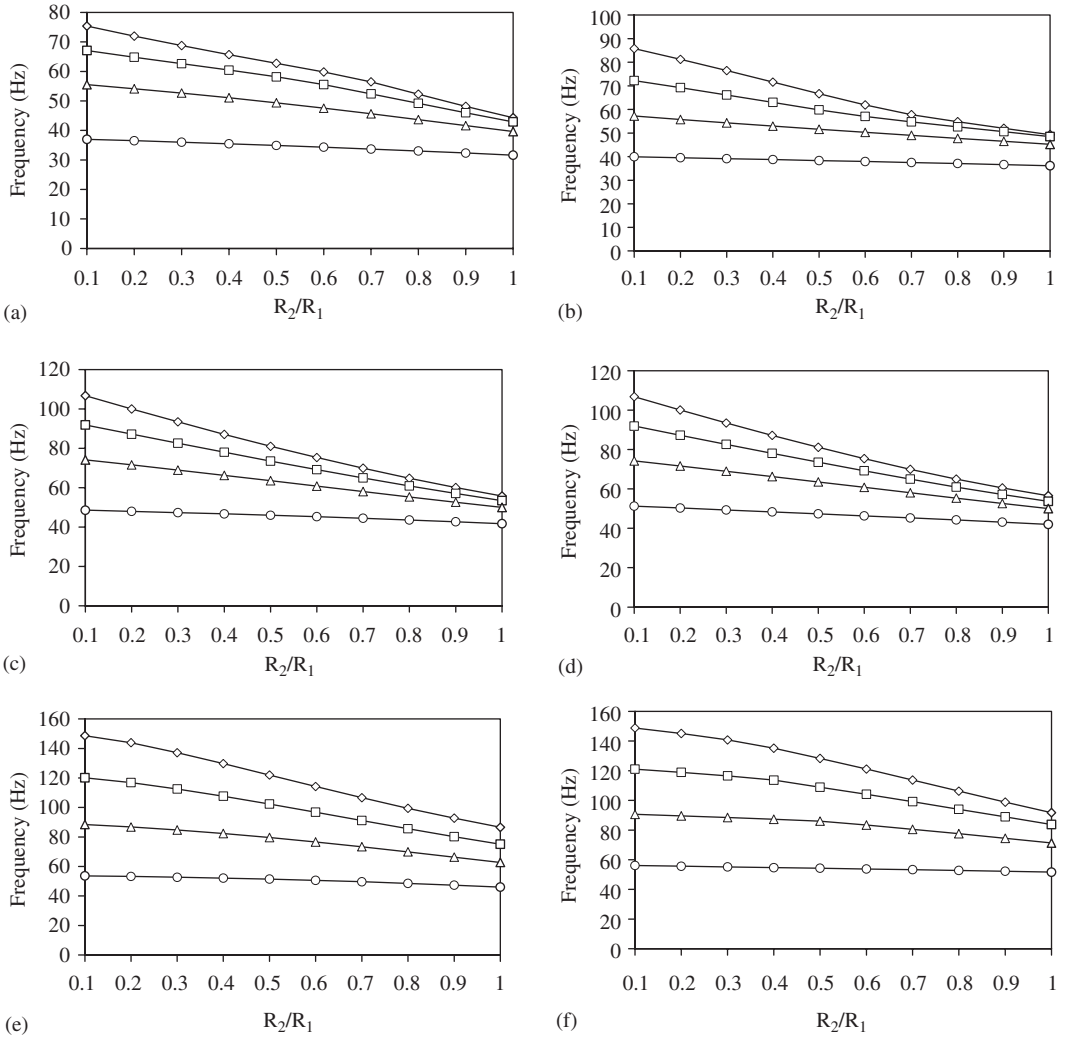

Fig. 6. Natural frequencies corresponding to: (a) first mode, (b) second mode; (c) third mode; (d) fourth mode; (e) fifth mode; (f) sixth mode for barrel type helices with ($\diamond$) $\beta = 1.00$, ($\square$) $\beta = 0.75$, ($\triangle$) $\beta = 0.50$, ($\circ$) $\beta = 0.25$.

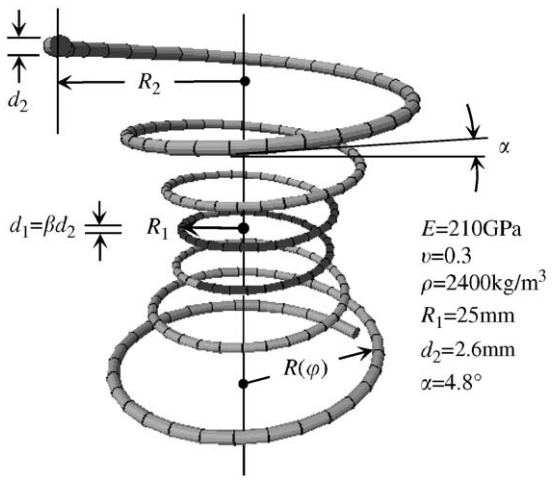

Fig. 7. Perspective view of hyperboloidal spring with variable circular cross-section.

4.2. Example 2—hyperboloidal helix

Geometrical and material properties of hyperboloidal helix (see Fig. 7) fixed at both ends are $R_2 = 13\,\text{mm}$, $n = 6.5$, $d = 2.6\,\text{mm}$, $\alpha = 4.8^\circ$, $E = 210\,\text{GPa}$, $\upsilon = 0.3$, $\rho = 7850\,\text{kg/m}^3$, $\alpha_n = \alpha_b = 1.1$ while R_1 is variable.

Constant cross-section case: The first six natural frequencies for the most extreme case ($R_1/R_2 = 2.4$) were verified by comparing with the results given by Nagaya et al. [10], Yildirim and Ince[16] and analyzed by ANSYS. The results were displayed in Table 3.

Variable cross-section case: The diameter of circular cross-sections is equal to $d_2 = 2.6\,\text{mm}$ at the points of $R = R_2$ and the diameter reduces linearly to βd_2 at $R = R_1$. Diameter variations were investigated for the concerning values of β. The extreme case, $R_1/R_2 = 2.4$, was also examined. Since it is an original example introduced to the literature the first six natural frequencies were only compared with ANSYS whose results were given in Table 4. It can be stated again that the presented study provides sufficient

Table 3
Natural frequencies (in Hz) of hyperboloidal type spring with constant circular cross-section ($d = 2.6\,\text{mm}$, $R_1/R_2 = 2.4$, N: number of elements)

Mod	Nagaya et al. (theoretical) [10]	Yıldırım–Ince [16]	ANSYS [22]			This study			
	$N = 78$	$N = 50$	$N = 100$	$N = 500$	$N = 1000$	$N = 100$	$N = 75$	$N = 50$	$N = 30$
1	76.00	75.80	78.60	75.99	75.82	76.94	78.88	78.03	78.52
2	96.00	96.15	97.73	95.71	95.63	96.77	97.70	97.19	91.28
3	103.00	103.07	107.30	103.90	103.64	105.38	108.96	106.19	93.09
4	133.00	132.85	135.93	132.73	132.56	134.43	135.90	135.12	127.76
5	—	160.69	163.61	159.78	159.60	161.62	163.60	162.30	153.70
6	—	182.96	190.30	184.39	184.03	186.49	189.81	188.32	156.30

Table 4
Natural frequencies (in Hz) of hyperboloidal type spring with variable circular cross-section ($d_2 = 2.6\,\text{mm}$, $d_1 = \beta d_2$,$R_1/R_2 = 2.4$, N: number of elements)

β	Mod	ANSYS [22]			This study			
		$N = 100$	$N = 500$	$N = 1000$	$N = 100$	$N = 75$	$N = 50$	$N = 30$
	1	82.44	79.83	79.67	80.81	82.61	81.85	82.71
	2	103.01	100.67	100.55	101.86	103.40	102.32	94.94
0.75	3	109.37	106.36	106.15	107.80	110.70	108.43	96.18
	4	134.18	130.92	130.74	132.57	133.35	133.35	130.37
	5	155.81	151.13	150.84	153.07	154.42	154.42	148.31
	6	165.13	160.53	160.28	162.41	163.81	163.81	157.66
	1	87.21	84.57	84.41	85.56	87.25	86.51	87.49
	2	109.72	107.10	106.94	108.39	110.40	108.78	99.05
0.50	3	111.53	108.73	108.54	110.12	112.56	110.58	99.86
	4	133.77	130.45	130.27	132.02	133.55	132.78	131.84
	5	138.20	134.04	133.79	135.71	138.28	136.99	135.77
	6	151.81	147.37	147.11	149.31	153.19	150.62	145.68
	1	92.73	90.05	89.90	91.01	92.47	91.67	92.09
	2	111.60	108.33	108.13	109.67	112.16	110.56	103.44
0.25	3	118.52	115.74	115.56	117.04	119.01	116.94	104.97
	4	123.24	120.39	120.22	121.71	123.31	121.70	116.97
	5	132.15	128.87	128.69	130.26	131.59	130.74	130.34
	6	145.54	141.13	140.84	143.00	146.98	144.03	133.42

consistency via 100 elements, while ANSYS needs much more elements. The first six natural frequencies were analyzed for $\beta = 0.25,0.50,0.75,1.00$ and $R_1/R_2 = 1.0,\ldots,2.4$ with the increment of 0.1 and illustrated in Fig. 8.

4.3. Example 3—conical helix with variable rectangular cross-section

Geometrical and material properties of a conical helix fixed at both ends (see Fig. 9) are $n = 2$, $R_1 = 7.50\,\text{m}$, $R_2 = 3.00\,\text{m}$, $b_1 = 2.50\text{m}$ (at $\varphi = 0$), $\alpha = 5.2^\circ$, $E = 30\,\text{GPa}$, $\upsilon = 0.15$, $\rho = 2400\,\text{kg/m}^3$ and $\alpha_n = \alpha_b = 1.2$. The width of the rectangular cross-section is variable with respect to $b(\varphi) = b_1 - 0.1\varphi$ (m) for $0 \leqslant \varphi \leqslant 4\pi$ and the height of cross-section $t = 0.3\,\text{m}$ constant along the helix axis. For the verification of this original example with regard to the literature, the software ANSYS is again employed. The results were shown in Table 5. Natural frequencies for the first six modes are in good agreement with ANSYS. The presented study via 75 elements provides sufficient consistency, while ANSYS predicts them by using much more elements.

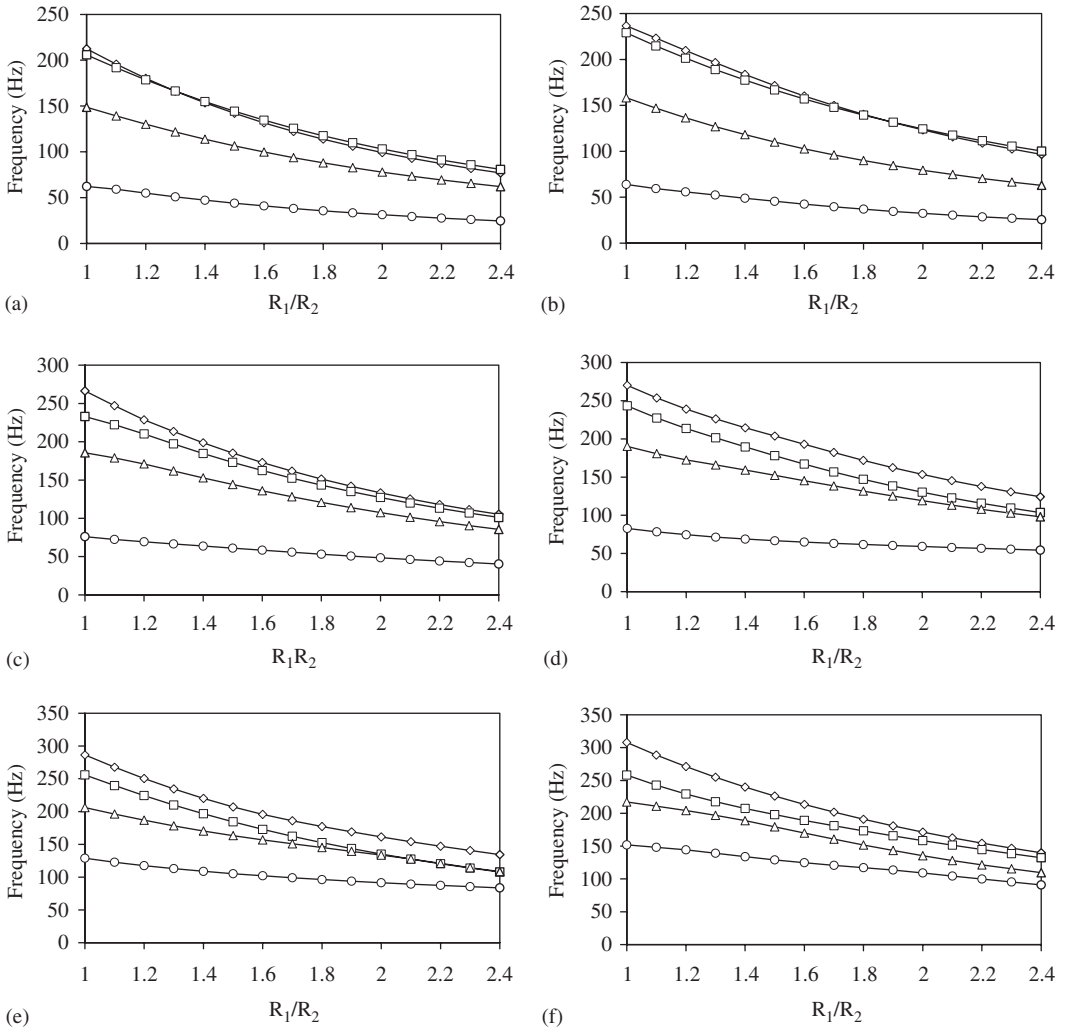

Fig. 8. Natural frequencies corresponding to: (a) first mode; (b) second mode; (c) third mode; (d) fourth mode; (e) fifth mode; (f) sixth mode for hyperboloidal type helices with ($\diamond$) $\beta = 1.00$, ($\square$) $\beta = 0.75$, ($\triangle$) $\beta = 0.50$, ($\circ$) $\beta = 0.25$.

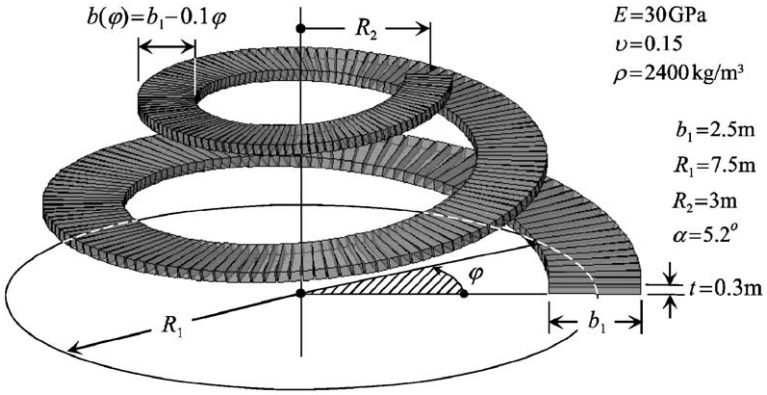

Fig. 9. Conical helix with variable rectangular cross-section.

Table 5
Conical helix with variable rectangular cross-section (N: number of elements)

Mod	ANSYS [22]				This study		
	$N = 50$	$N = 75$	$N = 100$	$N = 1000$	$N = 75$	$N = 50$	$N = 25$
1	0.4802	0.4785	0.4779	0.4772	0.4763	0.4763	0.4763
2	0.8140	0.8109	0.8098	0.8093	0.8116	0.8115	0.8107
3	1.4836	1.4768	1.4743	1.4737	1.4850	1.4847	1.4792
4	1.6879	1.6759	1.6712	1.6637	1.6622	1.6621	1.6595
5	1.9011	1.8909	1.8872	1.8830	1.8891	1.8886	1.8791
6	2.5733	2.5608	2.5563	2.5504	2.2571	2.2413	2.1595

5. Conclusion

In this study a mixed FE formulation, based on the functional [12,13], was developed for the free vibration analysis of non-cylindrical helices with variable cross-section. The mixed element and consistent mass matrices of helices, namely 3D curved bars, were derived according to the Timoshenko beam theory by including rotary inertia terms in the mass matrix and shear effects in the element matrix. Thus, the proposed method is also applicable to moderately thick bars and provides locking-free solutions. The geometry of non-cylindrical helices was approximated via a convenient approach capable to handle sophisticated geometries. The geometry approximation was carried out through the variable arc lengths and linear variations in curvatures via shape functions. The formulation was firstly verified with respect to precision and number of elements through the studies in the literature. In this study the original examples concerning non-cylindrical helices with variable cross-sections were contributed to the literature and verified by ANSYS. In fact, the results are in good agreement with the FE studies based on the exact geometry in the actual literature. The proposed method requires much less elements compared with FE programs employing straight bars.

As R_2/R_1 ratio of the barrel helices and R_1/R_2 ratio of the hyperboloidal helices decreases the natural frequencies of first six modes increase. Recalling Examples 1 and 2, β is a reduction factor for the cross-sectional diameter referring both types of helices. The higher β ratios, the higher natural frequencies. Dramatic increments in natural frequencies can be observed for high values of β ratios as well. In Example 1, for instance, in the case of $\beta = 0.75$, 0.50 and 0.25 for $R_2/R_1 = 0.20$, the reduction in first natural frequency compared with constant cross-sectional barrel helices corresponds to 9.91%, 24.77% and 49.24%, respectively. Similar behavior is valid for any R_2/R_1 ratio in barrel helices and any R_1/R_2 ratio in hyperboloidal helices (see Tables 1–4). Hence, a linear reduction at the cross-section up to the mid point of any helix will cause the natural frequencies to decline compared with the constant cross-section case.

Acknowledgements

The author gratefully acknowledges the excellent support provided by Professor Dr. Mehmet H. Omurtag. Results of this study are partially developed within a research project supported by the Research Foundation of ITU (Project No: 11_05_105).

References

[1] A.E.M. Love, The propagation of waves of elastic displacement along a helical wire, *Transactions of the Cambridge Philosophical Society* 18 (1899) 364–374.
[2] I. Epstein, The motion of conical coil springs, *Journal of Applied Physics* 18 (1947) 368–374.
[3] Y. Yoshimura, Y. Murata, *On the elastic waves propagated along Coil Springs*, Vol. 6(1), *Institute of Science and Technology*, Tokyo University, 1952.
[4] Y.F. Young, A.C. Scordelis, An analytical and experimental study of helicoidal girders, *Proceedings of American Society of Civil Engineering* ST1756 (1999).
[5] A.C. Scordelis, Internal forces in uniformly loaded helicoidal girders, *Journal of American Concrete Institute* 56 (1960) 1013–1026.
[6] V. Cinemre, Statical Analysis of Helical Rods by the Transfer Matrix Method, Ph Dissertation Thesis, Faculty of Civil Engineering, Istanbul Technical University, 1960 (in Turkish).
[7] W.H. Wittrick, On elastic wave propagation in helical spring, *International Journal of Mechanical Sciences* 8 (1966) 25–47.
[8] J.E. Mottershead, Finite elements for dynamical analysis of helical rods, *International Journal of Mechanical Sciences* 22 (1980) 267–283.
[9] J.E. Mottershead, The large displacements and dynamic stability of springs using helical finite elements, *International Journal of Mechanical Sciences* 24/9 (1982) 547–558.
[10] K. Nagaya, S. Takeda, Y. Nakata, Free vibration of coil springs of arbitrary shape, *International Journal of Numerical Methods in Engineering* 23 (1986) 1081–1099.
[11] D. Pearson, W.H. Wittrick, An exact solution for the vibration of helical springs using a Bernoulli-Euler model, *International Journal of Mechanical Sciences* 28 (1986) 83–96.
[12] A.Y. Akoz, M.H. Omurtag, A.N. Doğruoğlu, The mixed finite element formulation for three dimensional bars, *International Journal of Solids Structures* 28 (1991) 225–234.
[13] M.H. Omurtag, A.Y. Akoz, The mixed finite element solution of helical beams with variable cross-section under arbitrary loading, *Computers and Structures* 43 (1992) 325–331.
[14] Y. Xiong, B. Tabarrok, A finite element model for the vibration of spatial rods under various applied loads, *International Journal of Mechanical Sciences* 34/1 (1992) 41–51.
[15] V. Yıldırım, Investigation of parameters affecting free vibration frequency of helical springs, *Journal of Numerical Methods in Engineering* 39 (1) (1996) 99–114.
[16] V. Yıldırım, N. Ince, Natural frequencies of helical springs of arbitrary shape, *Journal of Sound and Vibration* 204 (2) (1997) 311–329.
[17] V. Yıldırım, Free vibration analysis of non-cylindrical coil springs by combined use of the transfer matrix and complementary functions methods, *Communications in Numerical Methods in Engineering* 13 (1997) 487–494.
[18] V. Yıldırım, Expressions for predicting fundamental natural frequencies of non-cylindrical helical springs, *Journal of Sound and Vibration* 252 (3) (2002) 479–491.
[19] J. Lee, D.J. Thompson, Dynamic stiffness formulation free vibration and wave motion of helical springs, *Journal of Sound and Vibration* 239 (2) (2001) 297–320.
[20] L.E. Becker, G.G. Chassie, W.L. Cleghorn, On the natural frequencies of helical compression springs, *International journal of Mechanical Sciences* 44 (2002) 825–841.
[21] W. Busool, M. Eisenberger, Free vibration of helicoidal beams of arbitrary shape and variable cross section, *Journal of Vibration and Acoustics, ASME* 124 (2002) 397–409.
[22] ANSYS**,** Swanson analysis systems, *Swanson J. ANSYS* 5.4. USA, 1997.
[23] M.H. Omurtag, *Strength of Materials*, Vol. 1, Birsen Publication, İstanbul, 2005. (in Turkish).
[24] S.P. Timoshenko, On the correction for shear of the differential equation for transverse vibration of prismatic bars, *Philosophical Magazine* 41 (1921) 744–746.